The Astrophysical Journal, 763:110 (8pp), 2013 February 1 doi:10.1088/0004-637X/763/2/110

ULTRA-DEEP *HUBBLE SPACE TELESCOPE* IMAGING OF THE SMALL MAGELLANIC CLOUD: THE INITIAL MASS FUNCTION OF STARS WITH $M \lesssim 1\ M_{\odot}$*

Jason S. Kalirai[1,2], Jay Anderson[1], Aaron Dotter[1], Harvey B. Richer[3], Gregory G. Fahlman[4], Brad M. S. Hansen[5], Jarrod Hurley[6], I. Neill Reid[1], R. Michael Rich[5], and Michael M. Shara[7]
[1] Space Telescope Science Institute, 3700 San Martin Drive, Baltimore, MD 21218, USA; jkalirai@stsci.edu, jayander@stsci.edu, dotter@stsci.edu
[2] Center for Astrophysical Sciences, Johns Hopkins University, Baltimore, MD 21218, USA
[3] Department of Physics & Astronomy, University of British Columbia, Vancouver, BC, Canada; richer@astro.ubc.ca
[4] National Research Council, Herzberg Institute of Astrophysics, Victoria, BC, Canada; greg.fahlman@nrc-cnrc.gc.ca
[5] Division of Astronomy and Astrophysics, University of California at Los Angeles, Los Angeles, CA 90095, USA; hansen@astro.ucla.edu, rmr@astro.ucla.edu
[6] Center for Astrophysics & Supercomputing, Swinburne University of Technology, Hawthorn VIC 3122, Australia; jhurley@swin.edu.au
[7] Department of Astrophysics, American Museum of Natural History, Central Park West and 79th Street, New York, NY 10024, USA; mshara@amnh.org
Received 2012 October 24; accepted 2012 December 4; published 2013 January 15

ABSTRACT

We present a new measurement of the stellar initial mass function (IMF) based on ultra-deep, high-resolution photometry of >5000 stars in the outskirts of the Small Magellanic Cloud (SMC) galaxy. The *Hubble Space Telescope (HST)* Advanced Camera for Surveys observations reveal this rich, cospatial population behind the foreground globular cluster 47 Tuc, which we targeted for 121 *HST* orbits. The stellar main sequence of the SMC is measured in the $F606W$, $F814W$ color–magnitude diagram down to ∼30th magnitude, and is cleanly separated from the foreground star cluster population using proper motions. We simulate the SMC population by extracting stellar masses (single and unresolved binaries) from specific IMFs and converting those masses to luminosities in our bandpasses. The corresponding photometry for these simulated stars is drawn directly from a rich cloud of 4 million artificial stars, thereby accounting for the real photometric scatter and completeness of the data. Over a continuous and well-populated mass range of $M = 0.37$–$0.93\ M_{\odot}$ (e.g., down to a ∼75% completeness limit at $F606W = 28.7$), we demonstrate that the IMF is well represented by a single power-law form with slope $\alpha = -1.90\ (^{+0.15}_{-0.10})$ (3σ error) (e.g., $dN/dM \propto M^{\alpha}$). This is shallower than the Salpeter slope of $\alpha = -2.35$, which agrees with the observed stellar luminosity function at higher masses. Our results indicate that the IMF does *not* turn over to a more shallow power-law form within this mass range. We discuss implications of this result for the theory of star formation, the inferred masses of galaxies, and the (lack of a) variation of the IMF with metallicity.

Key words: galaxies: photometry – galaxies: stellar content – Magellanic Clouds – methods: data analysis – methods: statistical – stars: luminosity function, mass function – techniques: photometric

Online-only material: color figures

1. INTRODUCTION

Understanding the initial mass function (IMF) of stars is one of the most important and sought after pursuits of astrophysics. The stellar IMF holds its origins in the theory of star formation, and is imprinted through physical processes such as turbulence, gravitational fragmentation of clouds, accretion in dense cores, and ejection of low-mass objects (Larson 1981; Bonnell et al. 2007). The physics of these processes can be constrained by measuring the shape and universality of the IMF in vastly different environments, such as metal-rich and dense star-forming regions in disks, metal-poor and sparse spheroid populations, and gravitationally bound star clusters. Additionally, the IMF serves as a key input to many interesting problems in astrophysics. The integral of the function at low masses ($\lesssim 1\ M_{\odot}$) determines the Milky Way mass budget including the number of substellar objects, the slope at intermediate masses ($\gtrsim 1\ M_{\odot}$) establishes the level of chemical enrichment into the interstellar medium, and the shape of the function at higher masses controls the amount of kinetic feedback that stellar populations impart to their surroundings. Ultimately, the IMF represents a key ingredient to general studies of distant galaxies by providing insights on the mapping between unresolved light from a mix of stellar populations to fundamental properties (e.g., star formation history and mass-to-light ratios).

There is a rich history of astronomical studies aimed at characterizing the IMF, as summarized in recent reviews by Chabrier (2003), Bastian et al. (2010), and Kroupa et al. (2011). The majority of previous investigations have calculated the distribution of masses from observations of stars near the Sun. Salpeter (1955) found that the smoothly varying luminosity function of these stars (from $M_V = -4$ to $+13$) was reasonably approximated by a power-law form with (slope) $\alpha = -2.35$ over a mass range of 0.4–10 $M_{\odot}$ (e.g., $dN/dM \propto M^{\alpha}$).[8] For $M \gtrsim 1\ M_{\odot}$, this initial work has been largely verified by subsequent analysis involving improved local stellar luminosity functions, although the exact shape of the IMF has been characterized by similar power-law slopes, log-normal distributions, or Gaussian distributions (e.g., Miller & Scalo 1979; Gilmore et al. 1985; Scalo 1986; Hawkins & Bessell 1988; Stobie et al. 1989; Scalo 1998; Kroupa et al. 1993; Kroupa 2001, 2002; Reid et al. 2002). At a characteristic mass that is $<1\ M_{\odot}$, several of these studies

* Based on observations with the NASA/ESA *Hubble Space Telescope*, obtained at the Space Telescope Science Institute, which is operated by the Association of Universities for Research in Astronomy, Inc., under NASA contract NAS5-26555. These observations are associated with proposal GO-11677.

[8] We adopt the convention of a "linear" slope for the IMF, where a Salpeter power law has $\alpha = -2.35$. This is equivalent to a logarithmic slope of $\Gamma = -1.35$.

have reached the conclusion that the IMF flattens. For example, Kroupa et al. measure a break in the IMF slope at 0.5 $M_{\odot}$ from $\alpha = -2.3$ to $\alpha = -1.3$.

IMF studies that are based on the local luminosity function offer both advantages and disadvantages over alternative methods. The most robust data come from stars within a few tens of parsecs, where distances are well measured from parallaxes and binarity is resolved. However, limited sample sizes lead to strong statistical errors over specific regions of the IMF we seek to constrain. Expanded samples of disk stars are available from wide-field photometric surveys, but the resulting luminosity functions suffer from strong Malmquist bias and disagree with the nearby sample unless detailed corrections are made (see, e.g., Kroupa 1995 and Reid & Gizis 1997 for discussions). Other methods to measure the IMF include modeling the luminosity functions of star-forming regions, young star clusters, and old clusters. The nature of these stellar systems as simple populations offers a tremendous advantage over field studies. Over a wide spectrum of mass, the constituent stars share incredible similarities in their (well-measured) properties. Unfortunately, derivation of the IMF from such populations is affected by a different set of errors that are often difficult to assess (e.g., photometric uncertainties due to high levels of extinction in star-forming regions, membership errors due to field interlopers in more sparse populations, and mass-segregation effects in dynamically relaxed older clusters). Further discussion of recent measurements of the IMF from clusters is provided in the review by Bastian et al. (2010).

We present a new derivation of the stellar IMF based on high-precision *Hubble Space Telescope* (*HST*) photometry and astrometry of the outskirts of the Small Magellanic Cloud (SMC). The population represents an independent tool to bear on the study of the IMF, and offers several advantages over previous studies. First, photometry above the 75% completeness limit extends from $F606W = 22.6$ to 28.7 and includes >5000 stars on the unevolved main sequence, thereby providing a high-resolution mapping of the complete stellar mass distribution between $M = 0.37$–$0.93\,M_{\odot}$. Second, the population forms a tight sequence on the color–magnitude diagram (CMD) similar to a star cluster, and is therefore approximately cospatial and also only contains a small metallicity spread. Population members are selected from high-precision proper motions. Finally, the field SMC stars are well mixed dynamically, so the present-day mass function can be assumed to be consistent with the IMF.[9]

2. OBSERVATIONS AND DATA REDUCTION

The primary science goal motivating these observations was to characterize the complete stellar populations of the nearby Milky Way globular cluster 47 Tuc, in order to derive the cluster white dwarf cooling age (B. M. S. Hansen et al. 2013, in preparation). However, the line of sight through 47 Tuc also intersects the outskirts of the SMC dwarf galaxy. At the location of the specific 47 Tuc field, $\alpha = 00{:}22{:}39$ and $\delta = -72{:}04{:}04$, the stellar populations surveyed in the SMC are ∼2.3 deg (2.4 kpc) west of the galaxy center.

The observations were obtained over 121 orbits of exposure time with *HST* and the Advanced Camera for Surveys (ACS) in GO-11677 (PI: H. Richer). We obtained 117 exposures in $F606W$ (163.7 ks) and 125 exposures in $F814W$ (172.8 ks). These two filters provide superb sensitivity at optical wavelengths, and are ideally suited for high signal-to-noise ratio photometry of the SMC main sequence. The imaging field was observed at 13 different orientations, each separated by ∼20 deg, and is therefore well dithered to enable resampling of the point-spread function (PSF). The effective angular size of the observations is $5\farcm25 \times 5\farcm25$.

The data reduction for these observations is described in detail in Kalirai et al. (2012). Briefly summarizing, we first corrected all of the images for charge transfer inefficiency using the pixel-based corrections from Anderson & Bedin (2010). We then generated distortion-free images using MultiDrizzle (Fruchter & Hook 1997), and calculated transformations between each of these images to link them to a reference frame in each filter. The transformations were based on Gaussian-fitted centroids of hundreds of stars on each image (e.g., 47 Tuc and SMC stars), and the solution was refined through successive matches. The final offsets provide alignment of the individual images to better than 0.01 pixel. A second pass of MultiDrizzle was performed on the aligned images to flag cosmic rays and hot pixels. For this step, the sky background was calculated for each individual image and offsets were made to normalize the values. A third pass of MultiDrizzle was executed on the clean images to create supersampled stacks with a pixel scale of 0.03 arcsec, giving a PSF with a full-width half-maximum (FWHM) of 2.7 pixels.

To measure the photometry and morphology of all sources, the stand alone versions of the DAOPHOT II and ALLSTAR photometry programs were used on the stacked images (Stetson 1987, 1994). The final catalog is based on first performing aperture photometry on all sources that are at least 2.5σ above the local sky, then deriving a PSF from ∼1000 high signal-to-noise ratio and isolated stars in the field, and finally applying the PSF to all sources detected in the aperture photometry list. The PSF was calculated using a multi-step iterative method that built up to allow for third-order polynomial spatial variations across the field. The final catalog contains sources that were iteratively matched between the two images, and cleaned to eliminate background galaxies with χ^2 and sharpness cuts from the PSF fitting.

The location of the specific field that we targeted in 47 Tuc was chosen to overlap a large number of archival *HST* calibration images. The average date of these data is 2004, so this presents a 6 year baseline over which proper motions can be measured. Positions of all stars in these archival data were derived, and cross-identified with the new 2010 observations. Over the baseline, the SMC population is clearly separated from the 47 Tuc population, as shown in Figure 1. Detailed information on the proper motion measurements, including studies of the bulk motions of 47 Tuc and the SMC, as well internal motions of individual stars within these populations, will be provided in future papers. Here, we use the proper motions to cleanly separate the SMC stellar population from both the foreground 47 Tuc stars and from any residual extragalactic contamination caused by faint (nearly unresolved) galaxies.

3. ANALYSIS

We derive the IMF through several steps. First, we measure the luminosity function of the SMC by isolating the stellar main sequence of the galaxy using the proper motions. Next, we generate simulations of this population. This is done by drawing masses from different IMFs, and interpolating the masses within a small grid of stellar isochrones (e.g., mass–luminosity relations) to yield magnitudes. These ages and metallicities

[9] We refer to the initial mass function as the distribution of stellar masses following the process of star formation. This is not to be confused with the "primordial" mass function at high redshift.

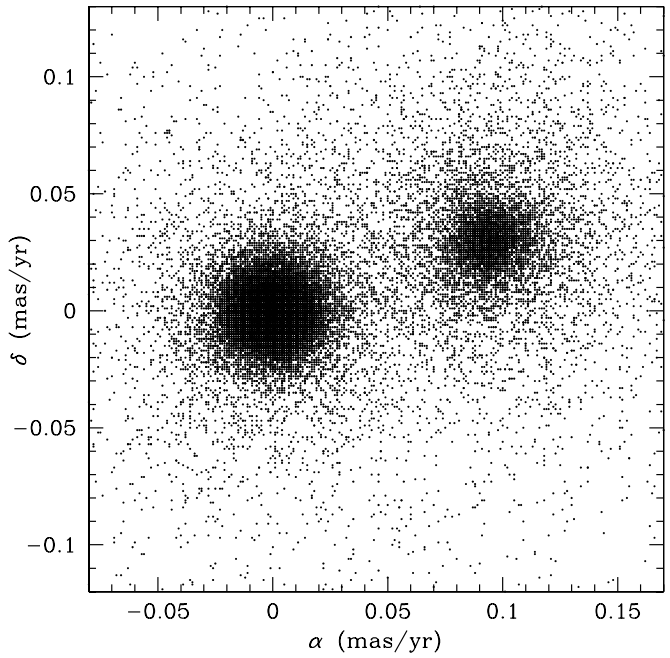

Figure 1. Proper motion distribution of stars along the sightline, based on a ∼6 year baseline between the present observations and a large number of *HST* archival images. The SMC population (right clump) is clearly separated from the cluster population.

Table 1
The SMC Luminosity Function

F606W	No. Stars (raw)	No. Stars (corr)
22.75 (±0.125)	89 ± 9	91.0 ± 9.7
23.00 (±0.125)	90 ± 9	92.2 ± 9.7
23.25 (±0.125)	93 ± 10	95.5 ± 9.9
23.50 (±0.125)	115 ± 11	118.5 ± 11.1
23.75 (±0.125)	147 ± 12	152.0 ± 12.5
24.00 (±0.125)	137 ± 12	142.2 ± 12.1
24.25 (±0.125)	154 ± 12	160.6 ± 12.9
24.50 (±0.125)	169 ± 13	177.4 ± 13.6
24.75 (±0.125)	166 ± 13	175.0 ± 13.6
25.00 (±0.125)	175 ± 13	185.5 ± 14.0
25.25 (±0.125)	184 ± 14	195.8 ± 14.4
25.50 (±0.125)	167 ± 13	179.2 ± 13.9
25.75 (±0.125)	189 ± 14	204.0 ± 14.8
26.00 (±0.125)	204 ± 14	222.3 ± 15.6
26.25 (±0.125)	190 ± 14	208.7 ± 15.1
26.50 (±0.125)	215 ± 15	238.3 ± 16.3
26.75 (±0.125)	207 ± 14	232.0 ± 16.1
27.00 (±0.125)	226 ± 15	256.4 ± 17.1
27.25 (±0.125)	272 ± 16	313.0 ± 19.0
27.50 (±0.125)	265 ± 16	311.4 ± 19.1
27.75 (±0.125)	294 ± 17	352.2 ± 20.5
28.00 (±0.125)	354 ± 19	433.5 ± 23.0
28.25 (±0.125)	422 ± 21	530.0 ± 25.8
28.50 (±0.125)	435 ± 21	564.6 ± 27.1

of these isochrones are chosen to match the CMD of the SMC population. This analysis includes careful consideration to ensure the simulated SMC population accounts for the photometric scatter and incompleteness of the real data. At this point, luminosity functions are constructed for the simulated main sequence and compared to the observations.

3.1. Isolating the SMC Stellar Population

Photometry of all stars along the sightline is illustrated in Figure 2. The CMD in the left panel reveals three populations of stars; the 47 Tuc main sequence (reddest stars), the SMC main sequence (middle), and the 47 Tuc white dwarf cooling sequence (bluest stars). In color–magnitude space, there is a mild separation between the latter two populations down to the faint limit of the data. This is illustrated in more detail in the small inset panel that focuses on the faint part of the CMD near $F606W = 29.25$. The darker points are selected as SMC members based on their proper motion (see Figure 1), and are reproduced in the middle panel on a finer scale down to $F606W = 28.6$ (this limit is discussed in Section 3.4).

The luminosity function of the SMC based on the selection described above is provided in Table 1. Both the raw counts from the confirmed members of the SMC and the completeness corrected star counts, based on the artificial star tests described below, are presented.

3.2. Metallicity, Distance, and Age

The complete SMC main sequence in this halo field is measured down to $F606W \gtrsim 30$. This is, therefore, the deepest investigation of the CMD of the galaxy to date. Previous wide-field photometric analysis of the field populations of the SMC suggest that the galaxy formed half of its stars >8 Gyr ago (e.g., Harris & Zaritsky 2004), and experienced more recent epochs of star formation in the main body. Surveys of the "halo" of the galaxy have characterized the bulk of the population as being old, although there are small differences in the measured star formation history among different regions (e.g., Graham 1975—a field near 47 Tuc; Dolphin et al. 2001; Nöel et al. 2007; Sabbi et al. 2009). Both photometric and spectroscopic studies across the halo of the SMC indicate evidence for a radial metallicity gradient (e.g., Sabbi et al. 2009; Carrera et al. 2008). In the western direction toward 47 Tuc at a distance >1.5 kpc, the metallicity of the population is [Fe/H] $\lesssim -1.1$ (Carrera et al. 2008).

To model the SMC population as a distribution of masses, we first compare the stellar main sequence on the CMD to a grid of moderately metal-poor stellar isochrones from the updated models of Dotter et al. (2008). Although the distance to the main body of the SMC is now precisely measured to be 60.6 ± 1.0 ± 2.8 kpc based on the analysis of 40 eclipsing binaries (Hilditch et al. 2005), there exists a significant depth to the galaxy of up to 20 kpc (Mathewson et al. 1988; Hatzidimitriou et al. 1993; Crowl et al. 2001; Lah et al. 2005; Haschke et al. 2012). Specifically, the eastern regions are closer than the western regions, so we expect the SMC population along our line of sight to have a larger distance than the main body. Fortunately, we can measure the distance to the population directly by using the unevolved fiducial of the bright 47 Tuc main sequence, a metal-poor population at $(m-M)_0 = 13.36 \pm 0.06$ (see Woodley et al. 2012, and references therein). By aligning the two sequences at $F606W = 24$–27, we derive the distance modulus of the SMC halo along this line of sight to be $(m-M)_0 = 19.1 \pm 0.1$. This calculation includes an offset of $\Delta(F606W) = -0.20$–0.30 to translate the [Fe/H] = −0.8 star cluster population to a range of SMC metallicities with $-1.4 <$ [Fe/H] < -1.0 (derived from the Dotter et al. models—see below). The uncertainty in the distance modulus is taken to be the small range over which we achieve acceptable fits of the two sequences, gauged by eye. The derived distance to the SMC population along this line of sight is in good agreement with the recent three-dimensional maps of

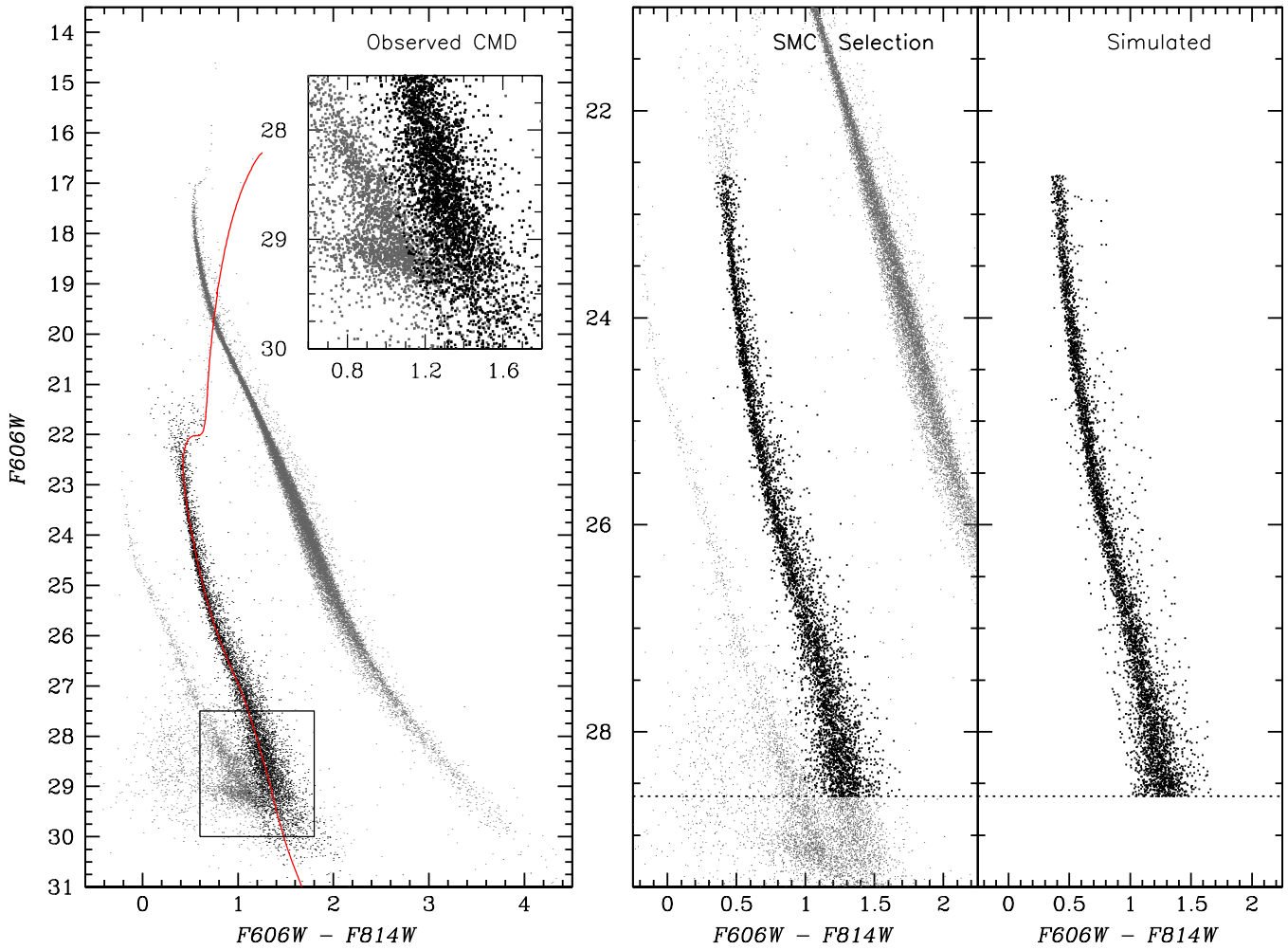

Figure 2. CMD of all stars along the line of sight in the *HST*/ACS observations (left). The photometry reveals three distinct populations; the main sequence and white dwarf cooling sequence of the foreground Milky Way globular cluster 47 Tuc (gray points), and the main sequence of the outskirts of the background SMC dwarf galaxy (e.g., the middle sequence—darker points). With a 50% completeness limit of $F606W = 29.9$ (see Section 3.3), this imaging represents the deepest probe of the SMC's populations to date. The inset panel presents a closer view of the faintest stars on the lower SMC main sequence (dark points) and 47 Tuc white dwarf cooling sequence (gray points). The red curve illustrates a stellar isochrone with [Fe/H] $= -1.1$ and $t = 7$ Gyr (Dotter et al. 2008), at a distance of $(m - M)_0 = 19.1 \pm 0.1$ (determined directly, as described in Section 3.2). The proper-motion selected SMC population, down to the limit of the data, is shown as darker points in the left panel, and reproduced down to $F606W = 28.6$ in the middle panel. As discussed in Section 3.4, we simulate the SMC population by drawing stars from an IMF and convolving them with (1) a range of mass–luminosity relations appropriate for the SMC halo, (2) binaries, (3) photometric scatter in the observations, and (4) incompleteness in the observations. An example of the simulated CMD, for an IMF with form $dN/dM \propto M^{-1.90}$, is shown in the right panel.

(A color version of this figure is available in the online journal.)

the SMC based on RR Lyrae stars (e.g., top-left panel of Figure 5 in Haschke et al. 2012).

In Figure 2, we illustrate a stellar isochrone with [Fe/H] $= -1.1$ and $t = 7$ Gyr superimposed on the observed SMC population. The isochrone is our best fit to the data, and nicely reproduces the main sequence, turnoff, subgiant branch, and red giant branch. According to this mass–luminosity relation, the faintest detected SMC stars at $F606W = 30.5$ have $M = 0.17\ M_{\odot}$. The "thickness" of the SMC main sequence indicates that the stellar population is both cospatial and contains only a small metallicity spread. For example, a direct comparison of the SMC sequence to that of 47 Tuc (a simple stellar population) on the same CMD indicates almost no additional broadening other than what is expected from photometric scatter (and binaries). Formally, we can rule out models with metallicities that fall outside of $-1.4 <$ [Fe/H] < -1.0 given the combined high-precision *HST* observations of the SMC lower main sequence and red giant branch. To account for this small metallicity spread in our derivation of the stellar IMF, our analysis below uses stellar isochrones (e.g., mass–luminosity relations) populated within this range.

Before continuing, we note that the age and metallicity of this remote population in a disturbed galaxy is interesting to study in its own right, for example, to establish the level of interaction-driven star formation and to constrain halo assembly models. The morphology of the main-sequence turnoff in the cleaned photometry of Figure 2 (left) shows multiple splittings, and so even this remote field of the SMC halo is not coeval. The brighter main-sequence turnoffs and subgiant branches extend to $F606W \sim 21.2$, with the most dominant population having $t = 4.5$ Gyr based on the same grid of stellar models. To avoid any biases from missing massive stars that have evolved in the younger populations, our analysis will only include stars on the SMC main sequence that are fainter than the oldest turn-off. At such old ages, the relation between mass and luminosity for these unevolved stars has a negligible dependence on age.

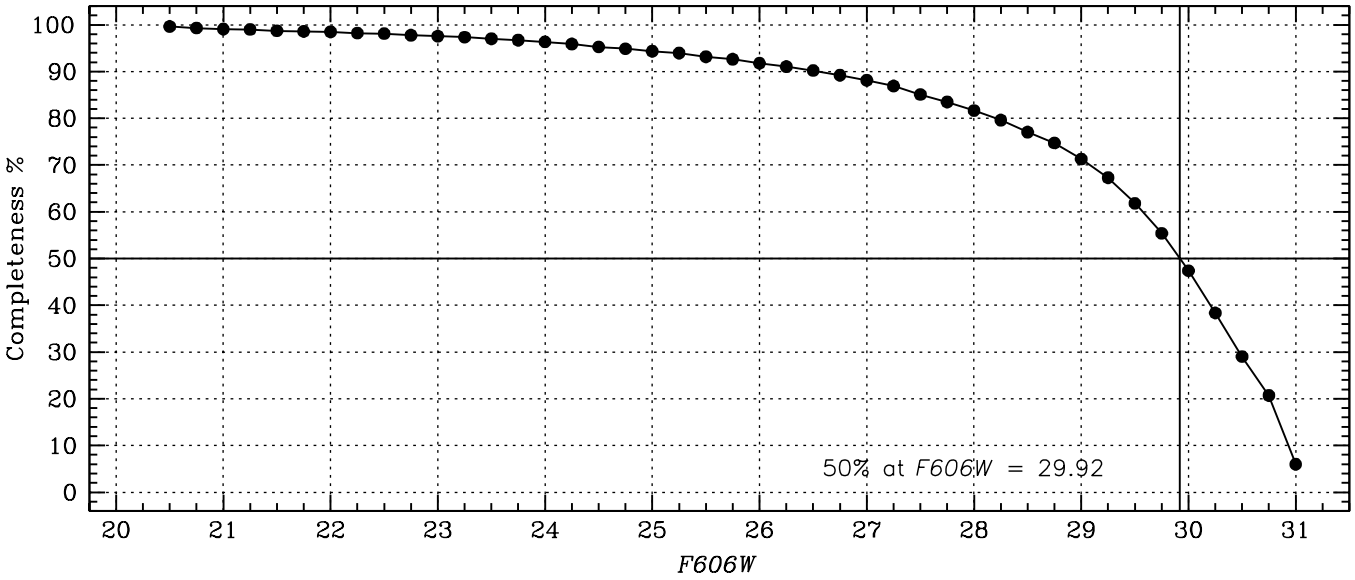

Figure 3. Completeness fraction of the artificial star test experiments on the *HST* images of the SMC population. As discussed in Section 3.3, input stars were placed on the SMC main sequence in the CMD and recovered blindly using the same photometric algorithms that were applied to the real data. A total 8000 trials were generated, with 4 million artificial stars (e.g., about ∼100,000 in each 0.25 mag bin). The 50% completeness limit of this data set, measured by requiring the star to be found in both filters, is $F606W = 29.9$.

3.3. Correcting Data Incompleteness

To measure the IMF from the distribution of stars along the SMC main sequence, we model the observations as a convolution of the input stellar masses, the mass–luminosity relation, and the selection functions in the data. We characterized the last by generating an extensive set of artificial star tests and analyzing these to constrain the data incompleteness and photometric errors. First, the stellar PSF was used to generate stars over the complete luminosity range occupied by real stars on the SMC main sequence (a flat luminosity function was used). These stars were injected into each of the $F606W$ and $F814W$ images simultaneously, with a color consistent with the observed SMC main sequence. The fraction of stars injected into each image was set to ∼1% of the total number of stars in the image, so as to not introduce incompleteness due to crowding in the tests themselves. A total of 8000 trials were generated, producing 4 million artificial stars.

Each of these new images, one per trial in each filter, were subjected to the same photometric routines that were applied to the actual drizzled images, using identical criteria. The stars were recovered blindly and automatically cross-matched between filters and to the input star lists containing actual positions and fluxes. Stars that were not recovered were also retained in the final matched lists and flagged as such. The end result of this process is a large scattering matrix that defines the fidelity of the observations and data reduction, including the photometric error distribution at any point in the CMD and the completeness. The 50% completeness limit of the SMC population in the joint $F606W$, $F814W$ CMD is $F606W = 29.9$ (see Figure 3).

We also assess whether the proper-motion selection imparts any additional incompleteness in the SMC population. An independent way to test this is to consider the stellar main sequence of 47 Tuc, which extends to beyond 30th magnitude in a region of color–magnitude space where there are no background galaxies. By comparing the luminosity functions with and without proper-motion selection, we confirm that there is no additional incompleteness down to at least $F606W = 29$, and possibly some very minor incompleteness fainter than this (e.g., much smaller than the data incompleteness itself).

3.4. The Initial Mass Function of Stars

We simulate the CMD in Figure 2 to derive the IMF through a multi-step process. First, random masses are drawn from a power-law IMF with a specific slope and populated within each of the five $-1.4 < [Fe/H] < -1.0$ stellar isochrones (e.g., see Figure 2 for the $[Fe/H] = -1.1$ model). For each bandpass, this provides luminosities for each mass at each metallicity. The results from the five metallicities are combined together with equal weighting. The simulation accounts for binaries by drawing a secondary companion star from the IMF for a fraction of the population, and setting the luminosity of the unresolved binary as the sum of the light from the two stars. The binary fraction among low-mass stars such as those in our study is 25%–35% (Leinert et al. 1997; Reid & Gizis 1997; Delfosse et al. 2004; Burgasser et al. 2007), and so we set the fraction to 30% in our simulation (see below). Next, for each mass in the input IMF, we randomly select stars from the $F606W$, $F814W$ artificial star cloud distribution if the luminosities associated with the input mass are consistent with the *input* magnitudes of a star in the cloud to 0.05 mag (in both filters). The luminosities that are extracted from the cloud are the *output* magnitudes of the matches. This method accounts for the photometric scatter and completeness of the data. The resulting simulated SMC CMD is shown in Figure 2 (right).

To measure the IMF, we compute the reduced chi square statistic (χ^2) between the luminosity function of each of the simulations and the SMC observations. The distribution of reduced χ^2 is shown in Figure 4, and exhibits a minimum at $\alpha = -1.90$ ($^{+0.15}_{-0.10}$) (3σ error). The χ^2 per degree of freedom is 0.86 for this IMF (e.g., $\chi^2 = 19.7$ for 24 degrees of freedom). The best-fit power-law form of the stellar IMF from these data is therefore $dN/dM \propto M^{-1.90}$, shallower than the Salpeter slope of $\alpha = -2.35$. A comparison of this derived IMF to the observed SMC luminosity function is shown in Figure 5, and demonstrates excellent agreement over the entire range of masses from

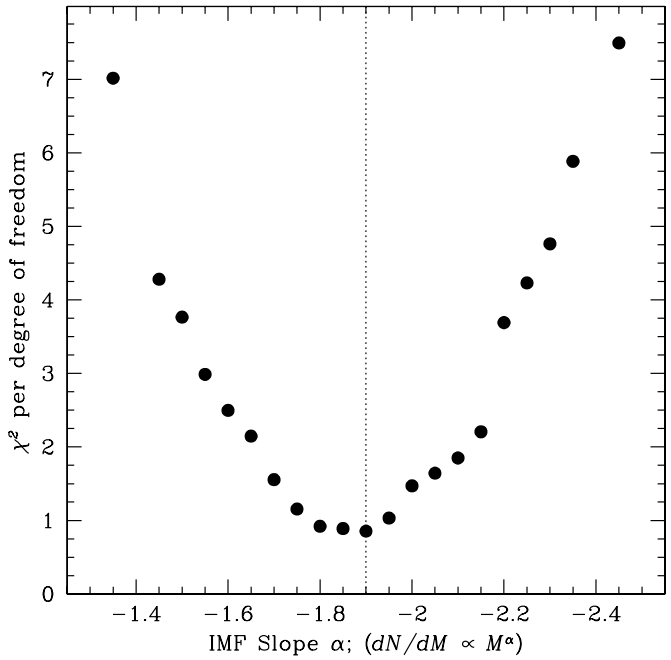

Figure 4. Distribution of χ^2 from the fit of power-law IMFs to the observed SMC luminosity function. The minimum occurs at $\alpha = -1.90\ (^{+0.15}_{-0.10})$ (3σ error), and the χ^2 per degree of freedom for this fit is 0.86.

$M = 0.37$–$0.93\ M_{\odot}$ (black curve). Figure 5 also illustrates two power-law IMFs with slopes that bracket the best-fit value as gray curves. This includes a shallower slope of $\alpha = -1.35$ (smaller counts at faint magnitudes) and the Salpeter slope of $\alpha = -2.35$, neither of which agrees with the data.

In this analysis, the observed luminosity function of the SMC is fit down to $F606W = 28.6$ (e.g., the limit shown in Figure 2). Below this limit, the data indicate some evidence for a turnover in the luminosity function that is inconsistent with an extension of this power law (e.g., the open circle points in the last two bins). It is difficult to constrain the slope of the mass function that matches these data given the limited leverage in stellar mass. Therefore, we stress that our primary result of an IMF with form $dN/dM \propto M^{-1.90}$ is only valid down to $M = 0.37\ M_{\odot}$, and should not be extrapolated to lower masses.

4. DISCUSSION

The derivation of the stellar IMF at $M < 1\ M_{\odot}$ gives a best-fit slope that is slightly shallower than a Salpeter IMF, which itself has had success in reproducing the observed luminosity function of nearby populations (the Salpeter 1955 result of $\alpha = -2.35$ is valid down to $M = 0.4\ M_{\odot}$). More importantly, the nature of our study provides excellent leverage to constrain the shape of the IMF over a *continuous* mass range with $M \lesssim 1\ M_{\odot}$, and is based on >5000 stars. Several previous studies have suggested that the IMF exhibits a "break" within this mass range. For example, the Chabrier (2003) log-normal IMF exhibits a shallow turnover in this mass range, the Kroupa (2001) power-law IMF indicates a slope change from −2.3 to −1.3 at $M = 0.5\ M_{\odot}$, and the Reid et al. (2002) analysis suggests that a break from a steeper IMF occurs at $M = 0.7$–$1.1\ M_{\odot}$. More recently, Bochanski et al. (2010) measured the IMF using multi-band photometry from the Sloan Digital Sky Survey (SDSS) over 8400 deg^2 (∼15 million stars), and found that the stellar distribution between $M = 0.32$–$0.8\ M_{\odot}$ is consistent with a single power law ($\alpha = -2.4$) and is significantly shallower

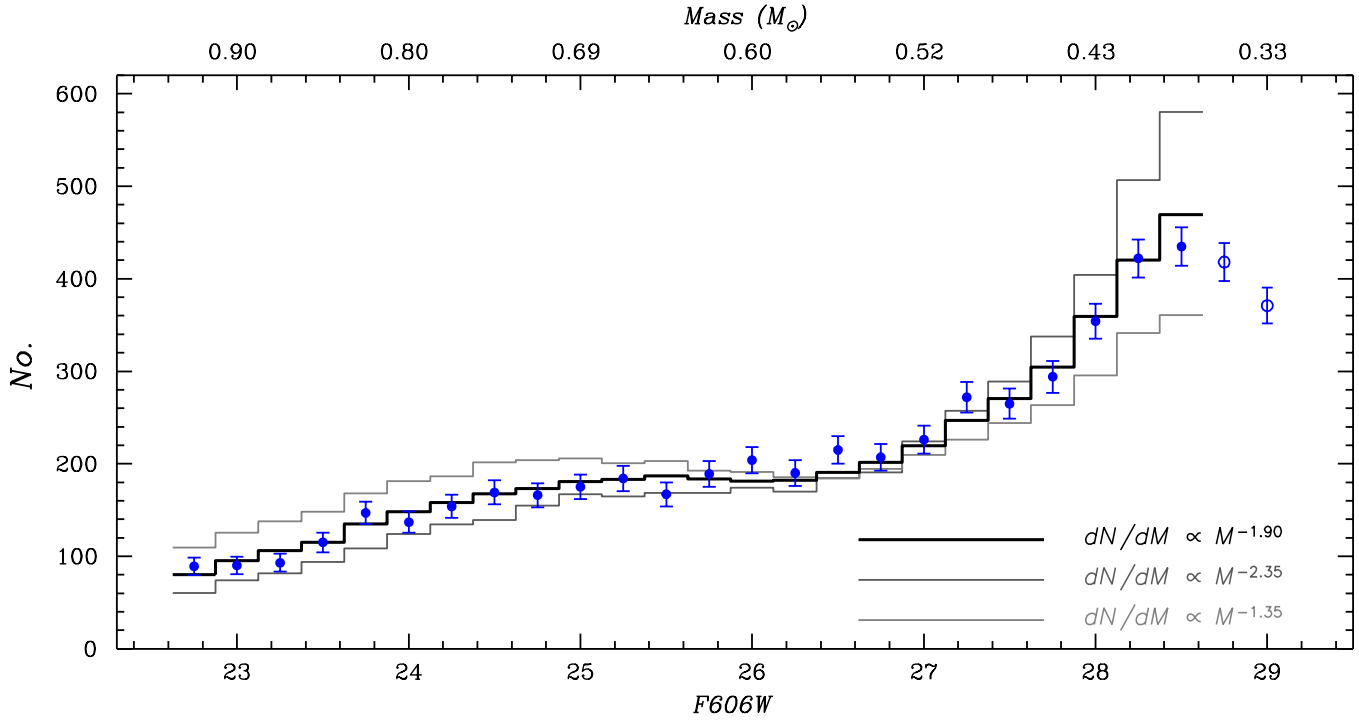

Figure 5. Deep luminosity function of the SMC from our *HST*/ACS observations is illustrated with blue points and error bars, along with three of the simulated luminosity functions based on different input IMFs (black and gray curves). The simulations are produced as described in Section 3.4. We obtain an excellent fit to the observations over the entire luminosity range extending from below the main-sequence turnoff to $F606W = 28.6$ with a single power law. The best-fit IMF slope over this range, from $M = 0.37$–$0.93\ M_{\odot}$, is $\alpha = -1.90$ (black curve). For comparison, the two gray curves illustrate IMFs with $\alpha = -1.35$ (lower counts at low masses) and −2.35 (the Salpeter IMF; higher counts at low masses). Fainter than $F606W = 28.6$, the observed SMC luminosity function shows a turnover which would not be reproduced by an extension of the $\alpha = -1.90$ power law.

(A color version of this figure is available in the online journal.)

at lower masses (e.g., or a log-normal distribution with $M_0 = 0.25\,M_\odot$).

The analysis of SMC stars with $M = 0.37$–$0.93\,M_\odot$ suggests that we do not require a two-component IMF to represent the data. A single power law is the simplest form of the stellar IMF, and it reproduces the observations nicely. Formally, if we fit a subset of the SMC population that only includes stars with $M > 0.60\,M_\odot$ (e.g., a cut at $F606W \lesssim 26$, the mid-point of the luminosity range), the best-fit slope is $\alpha = -2.05 \pm 0.3$ (with a much flatter χ^2 distribution). This is therefore in excellent agreement with our single power law over the full mass range. If we force a broken power-law fit, acceptable matches to the data are only obtained if the transition mass is shifted to fairly low masses $M < 0.5\,M_\odot$ *and* the difference in slope between the top and bottom ends is small (e.g., within ± 0.3 of $\alpha = -1.90$).

Many of the previous studies of the IMF that are based on local Milky Way field stars have relied on subsets of the same sample of stars. The present study is independent of these previous analysis, and of a very different nature. Our method takes advantage of a sample of SMC stars that are cospatial and that share similarities, yet it requires corrections to deal with binaries, photometric uncertainty, and completeness. Modest changes in the binary fraction do not affect our results. For example, we computed a separate set of IMFs with binary fractions of 20% and 40%, and found the best-fit IMF to the observed SMC luminosity function to be within ± 0.05 of the $\alpha = -1.90$ slope (the slope is steeper if the binary fraction is $\lesssim$10%). The completeness and photometric scatter is directly derived from an extensive set of artificial star tests as described in Section 3.3, and folded into our simulations to ensure no biases are introduced. Specifically, the SMC-selection from the CMD is very robust over the magnitude range adopted, and the completeness corrections are not large. Other systematics related to errors in the derived distance of the population or an error in the mass–luminosity relation of stars could have a minor impact on the slope of the derived IMF, but is unlikely to lead to a (large) systematic flattening of the slope over a specific mass range.

5. IMPLICATIONS

5.1. Theory of Star Formation

There are several implications of our result. First, studies of the IMF can constrain aspects of star formation theory. In one popular model, the mass distribution that is predicted from star formation is related to the efficiency of fragmentation in molecular clouds. Numerical simulations of turbulence and the resulting shock velocities (e.g., Larson 1979, 1981) indicate that the clump mass distribution is similar to a Salpeter-type (steep) IMF at $M \gtrsim 1\,M_\odot$ (Padoan & Nordlund 2002). Although the masses of the clumps continue to follow a power-law distribution down to lower masses (e.g., for scale-free turbulence), the IMF results from only those cores that are dense enough to collapse. The measurement of a slope for the IMF that is shallower than the Salpeter slope for $M = 0.37$–$0.93\,M_\odot$ (and yet shallower below this mass limit) suggests that a lower fraction of the low-mass cores suffered gravitational collapse and formed stars. This scenario suggests that the gas density in the molecular clouds is lower than what would be needed if the IMF continued at the Salpeter slope down to low masses (e.g., see models in Figure 1 of Padoan & Nordlund 2002).

Other star formation models involving gravitational fragmentation followed by a balance between accretion and dynamical ejection also predict specific shapes for the IMF. For example, Bate & Bonnell (2005) use hydrodynamical calculations to demonstrate that the characteristic mass of the IMF is dependent on the mean thermal Jeans mass of the clouds, $M_{\rm Jeans}$. Our finding of a shallower mass function at $M < 1\,M_\odot$ would be indicative of a higher $M_{\rm Jeans}$, and therefore less dense clouds relative to predictions from steeper IMFs (see Moraux et al. 2007 and references therein for further discussion). The exact impact of this finding depends critically on the shape of the IMF at masses that are lower than we measure here.

5.2. The Mass Budget of the Milky Way and M/L Ratios

Two of the most widely used applications of the IMF are to constrain the mass budget of the Milky Way and the mass-to-light ratios (M/L) of unresolved galaxies. Whereas higher mass stellar sources are responsible for the bulk of the energetics in galaxies and the light output, it is precisely the shape of the IMF at $M < 1\,M_\odot$ that dominates the inferred galaxy masses. Previous analysis has frequently adopted a Salpeter IMF over a broad mass range from 0.1–100 $M_\odot$ (e.g., outside the limits that it was constrained). For an old, simple stellar population, this leads to M/L ratios that are about a factor of two larger than the Chabrier IMF (e.g., see Chabrier 2003). For this generic example, our IMF would provide a M/L ratio that is lower than these IMFs given the shallower slope at intermediate masses, with the exact value being dependent on the assumption of the IMF at $M < 0.37\,M_\odot$. The full impact of the new IMF on understanding the properties of unresolved light from distant galaxies will require in-depth calculations in population synthesis techniques (e.g., Bruzual & Charlot 2003). As a related example, future estimates of the total mass of resolved populations from CMD analysis will be affected by our findings. As the lower mass stellar population is often undetected, an extrapolation with a single (shallower) power-law form down to $M = 0.37\,M_\odot$ will yield different stellar masses than a steeper IMF with a break at higher masses.

5.3. Metallicity Variations

Understanding any variation of the IMF with metallicity is fundamental, since $M_{\rm Jeans}$ depends on temperature and density, which in turn depend on processes that are linked to metallicity (e.g., cooling and dust emission). Despite many contrary remarks in the literature, the variation of the IMF with metallicity is poorly constrained. For example, the comparison of stellar luminosity functions in various star clusters with different metallicities requires specific corrections due to incompleteness in the data set and for the dynamical state of the particular cluster. Different investigators also use preferred sets of models and modeling techniques, thereby making it difficult to assess the systematic errors in the measurements. Recent work by van Dokkum & Conroy (2012) and Conroy & van Dokkum (2012) suggest that a true variation in the IMF does exist. Their work takes advantage of gravity sensitive absorption lines in the integrated light of old stellar populations of early type galaxies, where they find that galaxies with deeper potential wells have more dwarf-enriched mass functions (e.g., a more bottom-heavy mass function). Conroy & van Dokkum (2012) suggest that the IMF is steeper than a Salpeter IMF in early-type galaxies with the highest dispersions and [Mg/Fe].

The SMC stellar population offers a new opportunity to establish high-precision measurements of the IMF over an appreciable mass range with $M < 1\,M_\odot$, at a well-determined

metallicity. Our constraints on the stellar IMF from these data are derived directly from a luminosity function that includes between 100 and 450 stars in each 0.25 magnitude bin. The SMC population has $-1.4 < [Fe/H] < -1.0$, and is therefore an order of magnitude more *metal-poor* than solar neighborhood studies, yet an order of magnitude more *metal-rich* than the ultra-faint dwarf spheroidals. Two recent projects have measured the shape of the stellar luminosity function in each of these regions, and for stellar populations where dynamical corrections are not needed. First, at the metal-rich end, the IMF of the Galactic bulge was measured by Zoccali et al. (2000) using *HST*/NICMOS observations. Although their overall best fit for a single slope is $\alpha = -1.33 \pm 0.07$, this slope is affected by a turnover at the lowest masses. They point out that a two-slope IMF gives a better fit and has $\alpha = -2.00 \pm 0.23$ at $M > 0.5\,M_{\odot}$. Over the same mass range, we can also compare the luminosity function of the SMC (Table 1) to that of the Ursa Minor dwarf spheroidal galaxy which was studied by Feltzing et al. (1999) using *HST*/WFPC2. The distance to this galaxy is the same as the SMC, $(m - M)_0 = 19.1 \pm 0.1$, and the stellar population is both very old and metal-poor ([Fe/H] $= -2$). Feltzing et al. (1999) tabulate the star counts of this satellite, accounting for incompleteness, and demonstrate that the true luminosity function rises by a factor of 3.1 from $F606W = 23$ to 27 (e.g., above the 50% completeness limit). Over the same luminosity range, the SMC luminosity function in our data rises by a factor of 2.8 and is therefore in excellent agreement with the dwarf spheroidal results. Taken together, these studies demonstrate that the IMF is very similar in three unevolved and unrelaxed stellar populations with a large difference in metallicity of [Fe/H] $= >0$ to -2.0.

6. SUMMARY

Knowledge of the mass distribution of stars in stellar populations such as clusters and galaxies is a fundamental input to a wide range of problems in astrophysics. We have presented a new study of the IMF by analyzing high-precision *HST*/ACS photometry in one of the deepest images ever obtained for a nearby stellar population, the SMC. We isolate the SMC main sequence from the CMD and resolve a high-precision luminosity function of the galaxy down to 29th magnitude. This population is modeled by convolving input power-law IMFs with binaries, photometric scatter, and incompleteness. The best-fit IMF that reproduces the SMC population is $dN/dM \propto M^{-1.90^{+0.15}_{-0.10}}$ (3σ error), shallower than the Salpeter slope of $\alpha = -2.35$. We demonstrate that a single power law reproduces the completely mass distribution of stars from $M = 0.37$–$0.93\,M_{\odot}$, suggesting that the stellar mass function does not break in this range. At even lower masses, the data demonstrate a drop off in number counts that is inconsistent with an extrapolation of this IMF. A comparison of the SMC IMF at $-1.4 < [Fe/H] < -1.0$ to that of very metal-rich stars in the Galactic bulge, as well as very metal-poor stars in the Ursa Minor dwarf spheroidal galaxy, indicates a similar slope and therefore a negligible metallicity gradient.

We are grateful to Tom Brown for several useful discussions related to constructing artificial star tests and for simulating CMDs of stellar populations. We also thank Elena Sabbi for her help in providing background information on the SMC. Support for program GO-11677 was provided by NASA through a grant from the Space Telescope Science Institute, which is operated by the Association of Universities for Research in Astronomy, Inc., under NASA contract NAS 5-26555. H.B.R. is supported by grants from The Natural Sciences and Engineering Research Council of Canada and by the University of British Columbia.

Facility: HST (ACS)

REFERENCES

Anderson, J., & Bedin, L. R. 2010, PASP, 122, 1035
Bastian, N., Covey, K. R., & Meyer, M. R. 2010, ARA&A, 48, 339
Bate, M. R., & Bonnell, I. A. 2005, MNRAS, 356, 1201
Bochanski, J. J., Hawley, S. L., Covey, K. R., et al. 2010, AJ, 139, 2679
Bonnell, I. A., Larson, R. B., & Zinnecker, H. 2007, in Protostars and Planets V, ed. B. Reipurth, D. Jewitt, & K. Keil (Tucson, AZ: Univ. Arizona Press), 149
Bruzual, G., & Charlot, S. 2003, MNRAS, 344, 1000
Burgasser, A. J., Reid, I. N., Siegler, N., et al. 2007, in Protostars and Planets V, ed. B. Reipurth, D. Jewitt, & K. Keil (Tucson, AZ: Univ. Arizona Press), 427
Carrera, R., Gallart, C., Aparicio, A., et al. 2008, AJ, 136, 1039
Chabrier, G. 2003, PASP, 115, 763
Conroy, C., & van Dokkum, P. 2012, ApJ, 760, 71
Crowl, H. H., Sarajedini, A., Piatti, A. E., et al. 2001, AJ, 122, 220
Delfosse, X., Beuzit, J.-L., Marchal, L., et al. 2004, in ASP Conf. Ser. 318, Spectroscopically and Spatially Resolving the Components of the Close Binary Stars, ed. R. W. Hilditch, H. Hensberge, & K. Pavlovski (San Francisco, CA: ASP), 166
Dolphin, A. E., Walker, A. R., Hodge, P. W., et al. 2001, ApJ, 562, 303
Dotter, A., Chaboyer, B., Jevremovic, D., et al. 2008, ApJS, 178, 89
Feltzing, S., Gilmore, G., & Wyse, R. F. G. 1999, ApJL, 516, 17
Fruchter, A. S., & Hook, R. N. 1997, PASP, arXiv:astro-ph/9808087
Gilmore, G., Reid, I. N., & Hewett, P. 1985, MNRAS, 213, 257
Graham, J. A. 1975, PASP, 87, 641
Harris, J., & Zaritsky, D. 2004, AJ, 127, 1531
Haschke, R., Grebel, E. K., & Duffau, S. 2012, AJ, 144, 107
Hatzidimitriou, D., Cannon, R. D., & Hawkins, M. R. S. 1993, MNRAS, 261, 873
Hawkins, M. R. S., & Bessell, M. S. 1988, MNRAS, 234, 177
Hilditch, R. W., Howarth, I. D., & Harris, T. J. 2005, MNRAS, 125, 336
Kalirai, J. S., Richer, H. B., Anderson, J., et al. 2012, AJ, 143, 11
Kroupa, P. 1995, ApJ, 453, 350
Kroupa, P. 2001, MNRAS, 322, 231
Kroupa, P. 2002, Sci, 295, 82
Kroupa, P., Tout, C. A., & Gilmore, G. 1993, MNRAS, 262, 545
Kroupa, P., Weidner, C., Pflamm-Altenburg, J., et al. 2011, Stellar Systems and Galactic Structure, Vol. V (Berlin: Springer) (arXiv:1112.3340)
Lah, P., Kiss, L. L., & Bedding, T. R. 2005, MNRAS, 359, L42
Larson, R. B. 1979, MNRAS, 186, 479
Larson, R. B. 1981, MNRAS, 194, 809
Leinert, C., Henry, T., Glindemann, A., & McCarthy, D. W., Jr. 1997, A&A, 325, 159
Mathewson, D. S., Ford, V. L., & Visvanathan, N. 1988, ApJ, 333, 617
Miller, G., & Scalo, J. 1979, ApJS, 1, 513
Moraux, E., Bouvier, J., Stauffer, J. R., Barrado y Navascues, D., & Cuillandre, J.-C. 2007, A&A, 471, 499
Noël, N. E. D., Gallart, C., Costa, E., & Méndez, R. A. 2007, AJ, 133, 2037
Padoan, P., & Nordlund, A. 2002, ApJ, 576, 870
Reid, I. N., & Gizis, J. E. 1997, AJ, 113, 2246
Reid, I. N., Gizis, J. E., & Hawley, S. L. 2002, AJ, 124, 2721
Sabbi, E., Gallagher, J. S., Tosi, M., et al. 2009, ApJ, 703, 721
Salpeter, E. 1955, ApJ, 121, 161
Scalo, J. M. 1986, FCPh, 11, 1
Scalo, J. 1998, in ASP Conf. Ser. 142, The Stellar Initial Mass Function, ed. G. Gilmore & D. Howell (San Francisco, CA: ASP), 201
Stetson, P. B. 1987, PASP, 99, 191
Stetson, P. B. 1994, PASP, 106, 250
Stobie, R. S., Ishida, K., & Peacock, J. A. 1989, MNRAS, 238, 709
van Dokkum, P., & Conroy, C. 2012, ApJ, 760, 70
Woodley, K. A., Goldsbury, R., Kalirai, J. S., et al. 2012, AJ, 143, 50
Zoccali, M., Cassisi, S., Frogel, J. A., et al. 2000, ApJ, 530, 418